Hindawi
Advances in Civil Engineering
Volume 2019, Article ID 5343618, 10 pages
https://doi.org/10.1155/2019/5343618

Research Article

Vibration Failure of Young Low-Temperature Concrete Shaft Linings Caused by Blasting Excavation

Lidong Xie,[1,2] Zhaoxing Dong,[1] Yanjun Qi,[1] Ruohua Qiu,[1] and Qiang He[2]

[1]*School of Mechanics and Civil Engineering, State Key Laboratory for Geomechanics and Deep Underground Engineering, China University of Mining & Technology, Xuzhou 221116, China*
[2]*School of Civil Engineering, Xuzhou Institute of Technology, Xuzhou 221018, China*

Correspondence should be addressed to Zhaoxing Dong; mtdzx41@163.com

Received 6 September 2018; Revised 16 February 2019; Accepted 4 March 2019; Published 1 April 2019

Academic Editor: Constantin Chalioris

The freezing-blasting method constitutes the only available technique for excavating mining shafts within water-bearing bedrock. This study explores the effects of vibration damage to young C65 concrete shaft linings caused by close-range blasting excavation using the finite element method. C65 concrete test specimens were made in the laboratory and then cured at −7°C, and the elastic modulus, compressive strength, and longitudinal wave velocity were tested. The allowable dynamic tensile strength of the concrete for each mold of the shaft lining was obtained according to the observed strain rate of the concrete shaft lining using a regression formula. The finite element simulation results are basically consistent with the in situ measurements, thereby attesting to the validity of the numerical simulation. The blasting-induced vertical peak vibration velocity of the first mold of the concrete shaft lining reached 20~25 cm/s, which far surpasses the allowable vibration velocity range (i.e., 2~3 cm/s) in the Safety Regulations for Blasting for newly cast concrete between the initial setting and an age of 3 d. The tensile stress of the first concrete mold calculated by the finite element method is approximately equal to the theoretical tensile stress, both of which are smaller than the dynamic tensile strength of concrete. The cumulative energy sustained by the shaft lining of each mold and the allowable values of the dynamic tensile strength were obtained. The growth rate of the dynamic tensile strength of the subsequent molds was larger than that of the cumulative energy, and thus the safety of the shaft lining gradually improved. The C65 concrete would therefore not experience tensile failure after the shaft lining has sustained multiple rounds of blasting loads. This finding can provide a basis for safety considerations when employing the freezing-blasting method to construct mining shafts in water-bearing bedrock.

1. Introduction

Shallow coal resources are currently nearly drained. Consequently, it has become normal practice to construct shafts to depths over 500 m [1]. To accommodate such depths, shaft linings have gradually adopted C60 and higher-strength concretes [2]. Numerous provinces throughout China, including Shaanxi, Gansu, Ningxia, and Inner Mongolia, boast rich coal resources characterized by a thick bedrock on the upper surface, water-bearing bedrock, fissure water in aquifers, and poor preliminary grouting conditions. The only method that can be employed to construct shafts under these geological conditions is the freezing-blasting method [3, 4]. The parallel construction and casting of concrete shaft linings and the excavation of shafts through blasting under low-temperature (i.e., frozen) conditions in the water-rich bedrock can lead to the failure of young low-temperature concrete shaft linings exposed to blasting vibrations. Water leakage often occurs in a few places throughout shaft linings constructed using this parallel construction method, imposing serious restrictions on the application of this approach.

By conducting model tests, Zhang et al. [5] concluded that blast-induced vibrations can increase the strength of concrete within 1-2 d and decrease the strength thereafter. Li et al. [6] used in situ measurements and numerical simulations to study the attenuation of the blasting load energy in shafts and discovered that the vibration velocity of the first

mold of the newly cast concrete linings exceeds the allowable standard. Wang [7] acquired field measurements to investigate the impacts of blasting on shaft linings. However, they failed to monitor the first mold of the shaft lining, which is the closest to the work face and consequently suffers the most severe blasting impact, due to safety limitations associated with blasting and the potential damage to equipment from blast debris. Shan et al. [8, 9] determined via a physical model test with a 1 : 15 similarity ratio that the damage suffered by a shaft lining is obviously cumulative based on changes in the ultrasonic wave velocities at monitoring points both before and after blasting. However, indoor model tests, which are confined by the size of the bunker, the blasting bearing capacity, and the limitations on the model size, are more prone to reflections of stress waves from boundaries than practical engineering endeavors, and the test data are also limited. In addition, it is difficult to control the similarity ratio in an indoor model test, and the errors associated with the difference in the scale cannot be ignored.

The finite element method has been increasingly employed to predict structural responses under blasting loads. The LS-DYNA explicit finite element program contains more than two hundred material models that are widely used to simulate the responses of reinforced concrete structures under blasting loads. To date, a number of studies on the roles and principles of blasting construction and the related effects on tunnel lining structures have been released. Using the finite element method, Yang et al. [10] found that the secondary shotcrete should be constructed at least 24 m away from the blasting face to avoid vibration-induced failure. Jiang and Zhou [11], Jiang et al. [12], and Ahmed and Ansell [13, 14] studied the maximum peak vibration velocity allowed by a structure in a secure state. Mitelman and Elmo [15] and Li and Hao [16] utilized a finite element numerical simulation to study spalling in concrete under a blasting load. All of these studies focused on comparisons between the extracted vibration velocities at measurement points and standard values to determine whether the structures suffered damage. However, this approach fails to sufficiently address two problems. First, the stresses calculated through the finite element method are compared with the related design values of the material strength to determine whether the structure is damaged. Second, this method does not analyze the structural failure caused by the cumulative effects of multiple rounds of blasting. In addition, studies on the impacts of blasting on shaft linings using the finite element method have not been reported, to the best of our knowledge. The finite element method can eliminate the boundary effects of indoor model tests, alleviate the difficulty associated with controlling the material similarity ratio, and compensate for the inability (i.e., due to safety limitations in coal mine production) to monitor the vibration-induced failure of the first mold of the shaft lining using field measurements.

Therefore, this study used the finite element method to study the vibration failure of a young low-temperature C65 shaft lining. The aim was to explore whether the first mold of the shaft lining closest to the blasting face is damaged under the impacts of blasting loads, whether the shaft lining is damaged due to the cumulative effects of multiple rounds of blasting, and whether it is appropriate for China's Safety Regulations for Blasting [17] to adopt the peak vibration velocity as a standard for judging the failure of C60 and higher-strength concretes. To achieve these goals, this study took a mine in Inner Mongolia [7–9] as the study object. The temperature of the lining during the in situ construction was approximately −7°C. Test blocks of young C65 concrete at this temperature were made in the laboratory, and their uniaxial compressive strength, elastic modulus, and longitudinal wave velocity were measured. Then, these parameters were input to a finite element model, and the results were compared with observations at the engineering site [7] and the results of an indoor model test [8, 9]. The allowable values of the dynamic tensile strength for concrete in each mold of the shaft lining were obtained by using the measured strain rate of the concrete in the shaft lining [7]. As the effective tensile stress of the concrete element extracted by using the finite element method was smaller than the allowable value of the dynamic tensile strength of concrete, it is concluded that the allowable vibration velocity in the Safety Regulations for Blasting [17] is too conservative. The concrete shaft lining at an age of 1 d would not be damaged when the peak vibration velocity was <25 cm/s. Under the action of cyclic loads (an interval ≥ 2.5 d), the growth rate of the dynamic tensile strength of the subsequent molds of the shaft lining was greater than that of the cumulative energy, and thus the safety of the shaft lining improved gradually with the addition of molds, and the concrete comprising the shaft lining was not subject to tensile damage after multiple rounds of loading. If cracks and seepage occurred in the shaft body, the factors related to blasting construction could be excluded. The results of this study may have some reference and guidance values for blasting scheme formulation and the determination of blasting cycles in similar engineering backgrounds. Furthermore, this study may provide a background example for the amendment of the allowable velocity to ensure the safety of high-strength concrete shaft linings.

2. Materials and Methods

2.1. Project. The concrete shaft lining and external rock wall structure of the Inner Mongolian coal mine [7–9], the construction of which was achieved by adopting the freezing-blasting method, are shown in Figure 1, in which the X axis represents the radial direction and the Y axis represents the axial direction of the shaft. The origin of the coordinate system is the contact position between the rock mass and the outer surface of the first mold section of the shaft lining. The distance from the base of the first mold section of the shaft lining to the tunnel face was 4 m, and the diameter of the shaft body was 10.9 m. The undercover-reverse-building method was adopted to construct the external concrete lining, which was composed of C65 concrete, in tandem with the heading face. The cycle of each mold took 2.5 d, and the

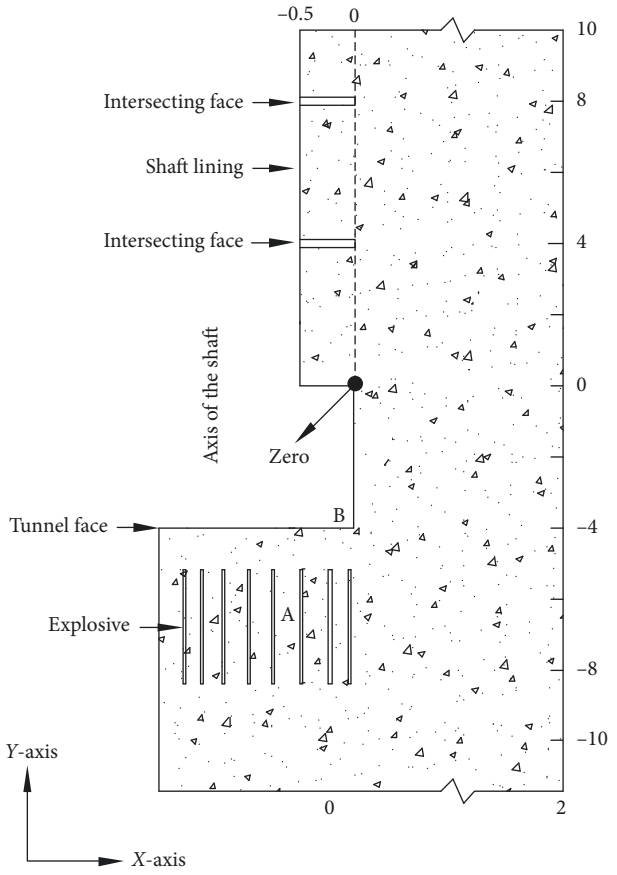

Figure 1: General model of the shaft wall (cm). Note: the directions and proportions of the X and Y axes are different. The scale along the X axis is not the same as that along the Y axis.

cyclical footage was 4 m. The axial height of the first mold spanned the interval of [0, 4] m, the radial thickness of the shaft lining spanned the interval of [−0.5, 0] m, the radial tunneling depth of the mold section covered the interval of [−8, −4] m, and the interval of the radial thickness of the external rock wall was [0, 2] m. The blasting hole was 4.5 m deep, with a diameter of 55 mm. The cylindrical charging center was radially located at −6.4 m. Electric detonators with 0, 25, 50, 75, and 100 ms delays were selected, and T220 rock water-gel explosives with a diameter of 45 mm and a cartridge length of 400 mm were adopted. The blasting parameters are shown in Table 1.

This study explored both the impacts of the blasting loads on the external concrete wall and the cumulative effects of multiple rounds of blasting impacts on the shaft lining. The excavation for each mold required 2.5 d. The interval between the completion and casting of a preceding mold section and the subsequent blasting time was 1 d. Eight molds of the shaft lining were sampled. The shaft lining and the external rock wall are magnified in Figure 2, and the concrete ages for each mold of the shaft lining are indicated on the right side of the figure.

2.2. Mechanical Properties of the C65 Concrete Material Used for the Shaft Lining. Test blocks with cubic dimensions of 100 mm × 100 mm × 100 mm [18] were made in the laboratory, cured for 12 h in a −7°C freezer according to the temperature conditions of the site and then taken out of the mold. The static uniaxial compressive strength, elastic modulus, and longitudinal wave velocity of each block were measured at room temperature, and the results are shown in Table 2.

The uniaxial compressive strength, elastic modulus, and longitudinal wave velocity parameters corresponding to the age (3.5, 6, 8.5, 11, 13.5, 16, and 18.5 d) of the concrete in each mold were obtained through smooth curve interpolation from known (i.e., measured) data, and the results are shown in Table 2. Poisson's ratio was assigned a constant value of $\mu = 0.22$, and the elastic modulus E, shear modulus G, and Poisson's ratio μ all satisfied the following equation:

$$G = \frac{E}{2(1+\mu)}. \tag{1}$$

The calculated results of the shear modulus of concretes of different ages are also shown in Table 2.

It is difficult to directly measure the dynamic tensile strength of young concrete at a high strain rate. By combining laboratory tests and numerical simulations, Grote et al. [19], Grote et al. [20], Zhang et al. [21], and Li et al. [22] found that the strain rates of concrete test blocks generally range between 10^1 and $10^2\,s^{-1}$ and that the growth factor of the concrete tensile strength is between 1.5 and 2.0; the tensile strength increases rapidly in the (4–10) interval. The measured tensile strength of the test blocks was used to calculate the allowable dynamic tensile strength of the C65 concrete.

Concrete is sensitive to the strain rate; for example, the dynamic tensile strength of concrete increases with the strain rate. According to the indoor simulation test and field measurement results, the strain rate $\dot{\varepsilon}$ of the concrete in the first mold of the shaft lining exceeded $10\,s^{-1}$ under the blasting load. The increase factor T_{DIF} of the tensile strength was calculated according to Malvar's modified CEB formula [23]:

$$T_{\mathrm{DIF}} = \frac{\sigma_{\mathrm{td}}}{\sigma_{\mathrm{ts}}} = \begin{cases} 1, & \dot{\varepsilon} \le \dot{\varepsilon}_{\mathrm{stat}}, \\ \left(\dfrac{\dot{\varepsilon}}{\dot{\varepsilon}_{\mathrm{stat}}}\right)^{\delta}, & \dot{\varepsilon}_{\mathrm{stat}} < \dot{\varepsilon} \le 1.0\,s^{-1}, \\ \theta \cdot \left(\dfrac{\dot{\varepsilon}}{\dot{\varepsilon}_{\mathrm{stat}}}\right)^{1/3}, & \dot{\varepsilon} > 1.0\,s^{-1}, \end{cases} \tag{2}$$

where the quasistatic reference strain rate is $\dot{\varepsilon}_{\mathrm{stat}} = 1 \times 10^{-6}\,s^{-1}$, the application range of $\dot{\varepsilon}$ is $(1 \times 10^{-6} \sim 160)\,s^{-1}$, $\delta = 1/(1 + 8\sigma_{\mathrm{cs}}/\sigma_{\mathrm{c0}})$, $\lg(\theta) = 6\delta - 2$, σ_{cs} denotes the static compressive strength, and $\sigma_{\mathrm{c0}} = 10$ MPa is a reference value.

According to the measured strain rate of the concrete in each mold of the shaft lining, the calculations according to equation (2) are somewhat conservative, and the growth factor of the tensile strength is $T_{\mathrm{DIF}} = 4$.

Xu et al. [24] performed a regression analysis on the compressive strength and splitting strength of concrete

Table 1: Blasting parameters.

Diameter no.	Hole number	Diameter (m)	Angle (°)	Explosive quantity (kg)	Hole distance (mm)	Segment	Segment explosive amount (kg)
1	9	1.4	86	44.1	479	I	44.1
2	12	2.4	87	50.4	621	II	50.4
3	18	3.6	90	63	625	III	287.7
4	26	5	90	109.2	603		
5	33	6.4	90	115.5	608		
6	40	8	90	168	628	IV	325.5
7	45	9.6	90	157.5	670		
8	52	10.7	93	145.6	646	V	145.6

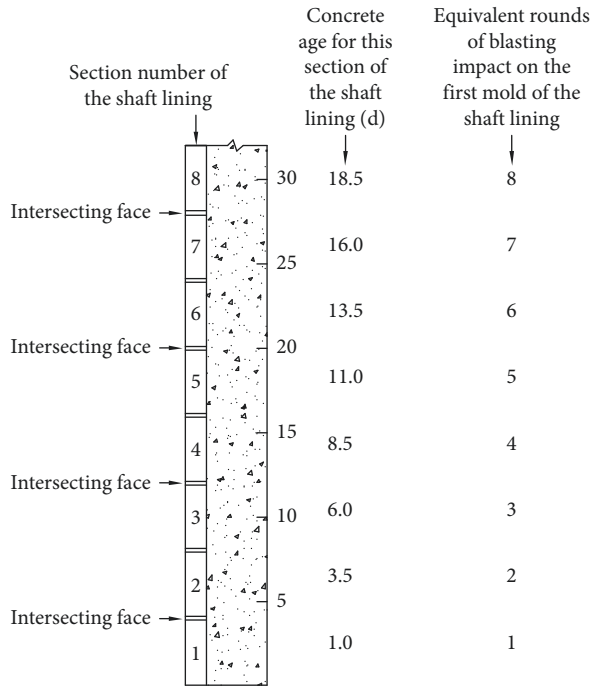

Figure 2: Schematic diagram of the shaft lining (cm).

cubes and derived the following formula according to the experimental data:

$$f_{t,s} = 0.1011 \cdot T_{DIF} \cdot f_{cu}^{0.9407}, \quad (3)$$

where $f_{t,s}$ is the splitting tensile strength and f_{cu} is the tensile strength of the testing block.

The tensile strengths of the C65 concrete cubes measured in the laboratory (shown in Table 2) were incorporated into equation (3) to calculate the splitting tensile strength. The resulting dynamic tensile strength of the C65 concrete sample in each mold is plotted in Figure 3, from which it is evident that the dynamic tensile strength tends to increase much more slowly beginning with the sixth mold (with an age of 13.5 d).

2.3. Material Models and State Equations

2.3.1. Explosive Model. The MAT_HIGH_EXPLOSIVE_BURN material was selected for the explosive, and the relationship among the internal energy, pressure, and relative volume during the detonation process is described by the Jones–Wilkins–Lee (JWL) state equation, as shown in the following equation:

$$p = A\left(1 - \frac{\omega}{R_1 V}\right)e^{-R_1 V} + B\left(1 - \frac{\omega}{R_2 V}\right)e^{-R_2 V} + \frac{\omega E}{V}, \quad (4)$$

where p is the detonation pressure, V is the volume of the detonation product generated by the charge in a unit volume, E denotes the internal energy of the unit volume detonation product, and A, B, R_1, R_2, and ω are the explosive parameters. The background engineering project adopted a T220 rock water-gel explosive, whose parameters are shown in Table 3 [25].

2.3.2. Air Model. The air element is described with the keyword MAT_NULL and the state equation LINEAR_POLYNOMIAL, as shown in the following equation:

$$P = C_0 + C_1\mu + C_2\mu^2 + C_3\mu^3 + \left(C_4 + C_5\mu + C_6\mu^2\right)E, \quad (5)$$

where P represents the pressure, E denotes the internal energy of a unit volume of air, and C_0–C_6 and μ are air material parameters, whose values are shown in Table 4.

2.3.3. Surrounding Rock Model. The kinematic hardening elastoplastic constitutive model, which is capable of describing the effects of the strain rate and kinematic hardening on the material, was adopted for the surrounding rock mass with the keyword MAT_PLASTIC_KINEMATIC. The background engineering project was a mine in Ordos where the typical rock mass in the mining area is a red sandstone, the parameters of which are shown in Table 5 [7, 25].

2.3.4. Concrete Model. The Holmquist–Johnson–Cook (HJC) material model was adopted for the concrete [26]. This model contains a yield surface equation (Figure 4(a)), a damage evolution equation (Figure 4(b)), and a state equation (Figure 4(c)).

The yield surface equation expresses a dimensionless equivalent stress, and the strain rate effect and the influence of material damage are considered. The equation is as follows [26]:

$$\sigma^* = \left[A \cdot (1 - D) + B \cdot P^{*N}\right]\left(1 + C \cdot \ln \dot{\varepsilon}^*\right), \quad (6)$$

Table 2: Mechanical parameters of C65 concrete test blocks of different ages.

Age (d)	1	2	3	3.5	6	7	8.5	11	13.5	14	16	18.5	28
Uniaxial compressive strength (MPa)	15.1	26	34.3	37.1	50.7	54.4	58.7	63	65.1	65.3	66.7	68.1	72.7
Elastic modulus (GPa)	22	26.5	30	30.4	33.7	34	34.9	35.5	35.8	35.8	35.9	36.1	36.3
Longitudinal wave velocity (m/s)	3125	3333	3571	3587	3808	3846	3925	4010	4073	4083	4123	4163	4267
Shear modulus (GPa)	9.2	11	12.5	12.7	14	14.2	14.5	14.8	14.9	14.9	15	15	15.1

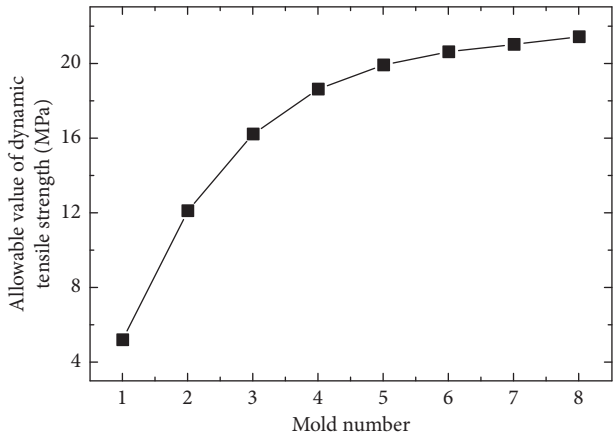

Figure 3: Dynamic tensile strength of C65 concrete in the different molds.

where $\sigma^* = \sigma/f_c$ and $P^* = P/f_c$ are the dimensionless equivalent stress and hydrostatic pressure, respectively, f_c is the static uniaxial compressive strength of the material, P is the actual hydrostatic pressure, $\dot{\varepsilon}^*$ is the ratio between the actual strain rate $\dot{\varepsilon}$ and the reference strain rate $\dot{\varepsilon}_0 = 1.0\,s^{-1}$, D is the damage factor ($0 \le D \le 1$), T^* is the dimensionless tension ($T^* = T/f_c$), T is the maximum tension stress the material can endure, S_{max} is the maximum dimensionless equivalent stress σ^* ($\sigma^* \le S_{max}$), A is the normalized cohesive strength, B is a normalized pressure hardening coefficient, N is a pressure hardening exponent, and C is a strain rate hardening coefficient.

Material damage is described by the accumulation of the equivalent plastic strain and plastic volumetric strain. The damage evolution equations are as follows [26]:

$$D = \sum \frac{\Delta\varepsilon_p + \Delta\mu_p}{\varepsilon_p^f + \mu_p^f},$$
$$\varepsilon_p^f + \mu_p^f = D_1\left(P^* + T^*\right)^{D_2} \ge \varepsilon_{f,min}, \quad (7)$$

where $\Delta\varepsilon_p$ and $\Delta\mu_p$ are the equivalent plastic strain and plastic volumetric strain within a single integral cycle, $\varepsilon_p^f + \mu_p^f$ is the plastic strain of material being crushed under a normal pressure, D_1 is a damage parameter of the model, and $\varepsilon_{f,min}$ is the minimum plastic strain at which the material is disrupted.

The state equation is composed of three parts. The first part involves the linear plastic range [26]. When $P \le P_{crush}$, the material is in a plastic state. The elastic bulk modulus $K = P_{crush}/\mu_{crush}$, where P_{crush} and μ_{crush} represent the pressure and volumetric strains in the uniaxial compression experiment. Within the elastic range, the loading and unloading state equation is as follows:

$$P = \frac{K}{\mu}. \quad (8)$$

The second part involves the plastic transition range. When $P_{crush} < P < P_{lock}$, the material remains in a plastic state. Within this range, as the pressure and plastic volumetric strains increase, the pores inside the concrete gradually shrink.

The third part involves the high-compression range. When $P \ge P_{lock}$, the material is under a high-compression state. Within this range, the relation between the pressure and the volume is as follows:

$$P = K_1\overline{\mu} + K_2\overline{\mu}^2 + K_3\overline{\mu}^3, \quad (9)$$

where $\overline{\mu} = (\mu - \mu_{lock})/(1 + \mu_{lock})$, K_1, K_2, and K_3 are constants, and $T(1 - D)$ represents the tension.

The parameters of the concrete are shown in Table 6 [7, 25] (showing concrete with an age of 1 d corresponding to the first mold of the shaft lining).

For the finite element model (shaft linings 2 through 8), among the parameters of the HJC material model, only E and f_c changed, while the other parameters remained constant. According to the age of the concrete of each mold of the shaft lining (see Figure 2), the parameters of each mold material were determined, and the results are shown in Table 2.

2.3.5. Calculation Model. Because of the symmetric structure of the shaft lining, only 1/4 of the model was studied. The net radius of the shaft body was 5.45 m, the radius of the external rock mass was 12 m, the height beneath the heading face was 8 m, and the height above the heading face was 36 m (8 casting mold sections). The bottom (i.e., lowest) concrete mold was 4 m from the heading face. To ensure that the finite element model was as similar to a practical engineering endeavor as possible, the fourth section (i.e., containing the maximum blasting charge) contained 4 blast holes, as shown in Figure 5. The explosive and air were defined according to ∗SECTION_SOLID_ALE (arbitrary Lagrangian–Eulerian) and calculated using the ALE multimaterial algorithm (this algorithm allows multiple materials to be transported within the same grid demarcated based on multimaterial elements); the shaft lining and the surrounding rock were defined according to ∗SECTION_SOLID and calculated using the Lagrangian algorithm; fluid-solid coupling among the surrounding rock, shaft lining, and air was performed in accordance with ∗CONSTRAINED_LAGRANGE_IN_SOLID. This calculation method has the following virtues: it allows fluid materials to flow within the Euler element, thus avoiding element distortions; furthermore, the employment of fluid-

Table 3: Material parameters of the T220 explosive [25].

ρ (g/cm^3)	D (m/s)	P_{cj} (GPa)	A (GPa)	B (GPa)	R_1	R_2	ω	E_0 (GPa)
1.2	5500	10	741	18	5.56	1.65	0.35	4

Table 4: Material parameters of air [25].

ρ (g/cm^3)	C_0	C_1	C_2	C_3	C_4	C_5	C_6	E (GPa)	V_0
1.29×10^{-3}	0	0	0	0	0.4	0.4	0	2.5×10^{-4}	1

Table 5: Material parameters of the red sandstone [7, 25].

ρ (g/cm^3)	E_1 (GPa)	M	σ_γ (GPa)	E_2 (GPa)	β	ε_f
2.1	1.8	0.2	0.08	0.18	0.5	0.06

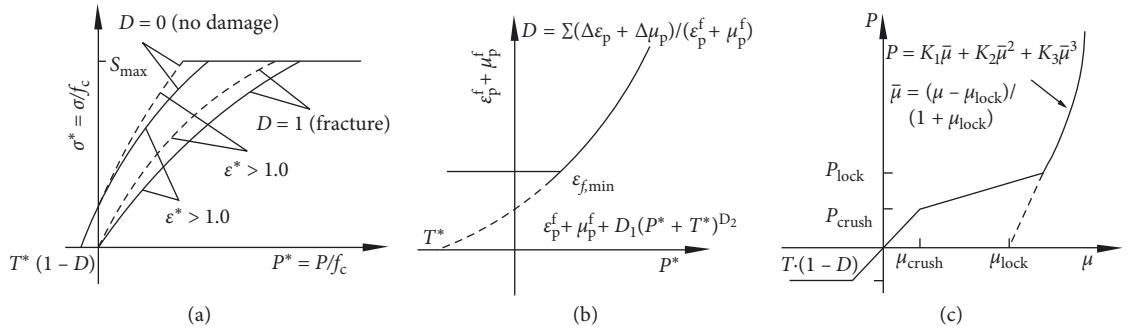

Figure 4: HJC concrete model. (a) Yield surface equation. (b) Damage evolution equation. (c) State equation.

Table 6: Material parameters of the concrete model [14, 25].

Parameter	Value
ρ (kg/m^3)	2400
f_c (MPa)	18.5
E (GPa)	33.1
v	0.2
T (MPa)	2
$\varepsilon_{f,min}$	0.01
S_{max}	7
A	0.79
B	1.6
C	0.007
N	0.61
P_{crush} (MPa)	16
μ_{crush}	0.001
P_{lock} (GPa)	0.8
μ_{lock}	0.1
D_1	0.04
D_2	1
K_1 (GPa)	85
K_2 (GPa)	−171
K_3 (GPa)	208

solid coupling to handle the interaction between solid and fluid materials provides a convenient way for the establishment of the blasting model [27]. In this study, the whole model contained 11 parts, with 53888 solid elements (the rock, 47744 elements; the eight-mold shaft lining constituted 6144 elements (768×8)) and 5600 liquid elements

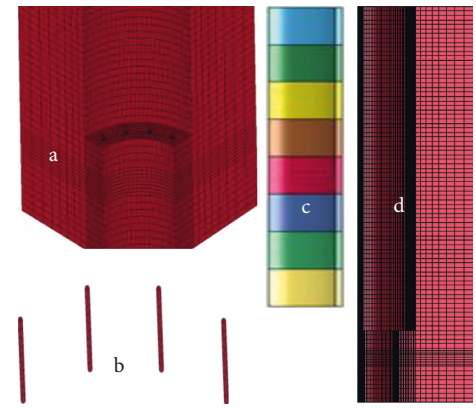

Figure 5: Finite element model of the shaft: (a) local magnification near the heading face; (b) magnification of the explosive grains; (c) eight molds of the shaft lining; (d) structure of the surrounding rock of the shaft body.

(the explosive, 480 elements; air, 5120 elements). To eliminate the impacts of reflected stress waves at the model boundaries on the simulation results, a symmetric constraint was applied to the two radial faces of the model. The surface within the shaft lining was a free boundary, and other radial faces were nonreflecting boundaries. In the finite element model, the blasting impact load sustained by the nth mold of the shaft lining was equivalent to the nth round of blasting load sustained by the first mold of the shaft lining.

3. Results and Discussion

The results of the field measurements [7], model tests [8, 9], and numerical simulation in this study all demonstrate that the axial vibration velocity at each measurement point in the shaft lining is the largest, followed by the radial velocity, and the tangential velocity is the smallest. The original shaft structure was a symmetrical, thin-walled cylinder, and thus the charge distribution was also symmetric. With regard to the blasting face, the free surface of the shaft was limited and resembled a cylindrical surface. The shaft material was composed of compact reinforced concrete, which inhibits the effects of vibrations; this is different from the characteristics of surface blasting, where the free surface is an infinite horizontal plane. These conditions caused the vibration velocities in the axial, radial, and tangential directions to exhibit the abovementioned results. Consequently, this study selected the axial vibration velocity of each mold of the shaft lining for further analysis. Each mold had a height of 4 m, and the bottom of the first mold was 4 m away from the heading face (Figure 1). The axial velocity was measured at seven measurement points [7] (corresponding to each point from the second mold to the eighth mold). The successive distances from the measurement points to the heading face were 9, 13, 17, 21, 25, 29, and 33 m. The axial velocities were measured during the indoor model test [8, 9] at three points (corresponding to two points on the first mold and one point on the second mold); the locations of those three points were then converted into distances (i.e., 5, 7, and 11 m) from the in situ shaft lining to the heading face. For the sake of comparison, the axial velocities of ten points with distances of 5, 7, 9, 11, 13, 17, 21, 25, 29, and 33 m from the heading face (corresponding to two points of mold 1 and mold 2 and one point of mold 3 to mold 8, respectively) were selected from the numerical model in this study. The relationships among the simulated values, test values, and in situ measured values are shown in Figure 6. Field measurements were not obtained for mold 1 (4 m to 8 m) due to factors of blasting safety. In indoor mold tests, molds 1 and 2 were cast, and molds 3 to 8 (13 m to 18 m) were not tested due to indoor factors. In contrast, the numerical simulation completed the tests on all molds.

As shown in Figure 6, with regard to the axial vibration velocity, the field measurements and mold tests had a small overlapping range with a great difference (where the vibration velocity ratio was between 1.3 and 1.4), although the variation trends were similar. To obtain a more accurate axial variation law, the results based on a third method were needed. The finite element method achieved this requirement satisfactorily: the trends of the three axial vibration velocities were consistent, thereby attesting to the credibility of the simulation results obtained by the finite element method. For the field measurements [7], sensors were attached to the outside of the shaft lining. However, the blasting vibration waves were reflected on the free surface, so the measured values were higher. For the indoor mold tests [8, 9], the sensors were embedded inside the shaft lining. Due to boundary effects, the reflected tension waves and compression waves from the upper boundary of the shaft

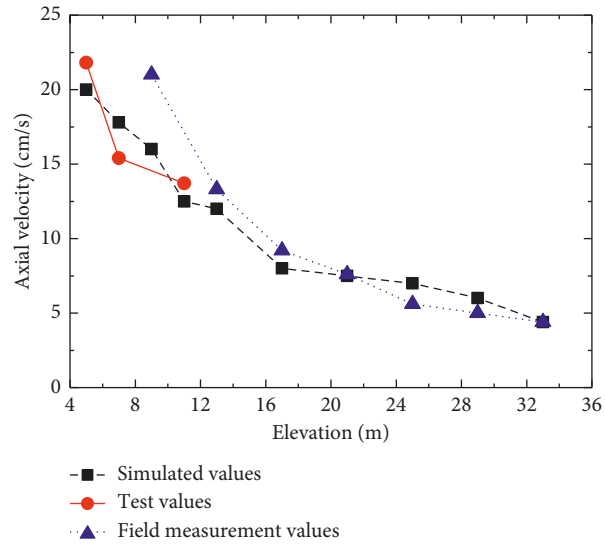

Figure 6: Axial vibration velocity comparison among molds of the shaft lining.

lining superimpose on each other. Furthermore, the similarity ratio between the materials was difficult to control. For these reasons, the measurement at the detected point on the first mold was lower than the actual value. The simulated values were in satisfactory agreement with the values obtained from the mold tests for molds 1 and 2 (4 m–12 m) and with those obtained from the field measurements for mold 3 to mold 8 (13 m–36 m). Furthermore, considering that the first mold was the most important in this study, the numerical simulation compensated for the failure to measure the in situ vibration velocity of the first mold of the shaft lining [7]. The extracted vertical peak vibration velocity of the first concrete mold reached 22 cm/s, which greatly exceeds the allowable vibration velocity (i.e., 2.0~3.0 cm/s) for newly cast concrete with general strength between the initial setting time and an age of 3 d according to China's Safety Regulations for Blasting. The first concrete model would therefore be damaged by the impact of a blasting load according to the abovementioned regulations. However, both field measurements and indoor mold tests showed a satisfactory structure for the shaft lining. Therefore, the allowable vibration velocity in the Safety Regulations for Blasting [17] is conservative for high-strength C65 concrete.

These results were obtained from a qualitative analysis of the safety of the structure of the shaft lining by measuring the axial peak vibration velocity under the action of blasting vibration. A quantitative analysis from the perspective of the stress was then performed.

The dynamic stress, wave impedance, and vibration velocity of the rock satisfy the following equation:

$$\sigma_d = \rho \cdot c \cdot V, \tag{10}$$

where σ_d is the dynamic stress of the rock material, $\rho \cdot c$ represents the wave impedance of the rock material, and V denotes the vibration velocity of the rock material.

The in situ vibration velocities of the abovementioned measurement points [7] and the vibration velocities of the

measurement points in the indoor model test [8, 9] were incorporated into equation (10) to solve for the tensile stress in the theoretical axial direction of the concrete. Subsequently, the effective tensile stress values in the axial direction for the abovementioned measurement points were extracted from the finite element model in this study. The relationships among the three sets of velocity data are shown in Figure 7.

As shown in Figure 7, the boundary effect is responsible for the smaller measured stresses in the indoor model test and the difficulty associated with controlling the material similarity ratio. The results of the finite element simulation are very similar to the in situ results, with errors less than 10%. The simulated values are slightly larger than the measured values, which is attributed to the presence of fissures and joints, which attenuate stress waves, in an actual rock mass. Therefore, it is safer to use the simulated values as the actual values of the tensile force sustained by the shaft lining, especially because the finite element simulation effectively compensated for the deficiency of the in situ field measurements given that the first mold closest to the heading face was not monitored during the field investigation. The effective vertical peak tensile stress extracted from the finite element simulation results was 2.25 MPa, whereas the allowable value of the dynamic tensile stress corresponding to the age of the first mold in the indoor model test was 5.2 MPa (Figure 3), and the safe allowable coefficient was 2.3. From mold 2 to mold 8, the distance from the explosion center increased and the tensile stress of the concrete decreased rapidly (Figure 7), whereas the allowable value of the dynamic tensile stress of the concrete of each mold increased (because of the increase in age; Figure 3). Therefore, the safety of the shaft lining gradually increased. These results demonstrate that the vibration velocities at the measurement points far exceeded the allowable values in the Safety Regulations for Blasting. In terms of the peak stress, the concrete shaft lining was still in a secure state, and it did not incur any damage. Therefore, the allowable peak particle velocities (PPVs) in the Safety Regulations for Blasting are too conservative for C60 or higher-strength concrete shaft linings. The above conclusions are also applicable to similar engineering endeavors [13, 14]. Consequently, although the PPVs of tunnel shotcrete support structures exceeding the allowable values in the Safety Regulations for Blasting, the structures are still secure.

However, the assessment of the safety of the shaft lining structure from the perspective of the tensile strength of the first mold cannot lead to a complete conclusion. As the shaft lining construction proceeds, each mold of the lining will endure the effects of the subsequent rounds of blasting loads. Therefore, the safety of the shaft lining under the cumulative tensile stress should also be considered. Although the finite element method cannot obtain the cumulative tension damage value of the concrete $\sum D$, this value is governed by the cumulative total energy E_t of each mold of the shaft lining, and the two values have a positive linear correlation. In this study, the cumulative energy E_t is used to directly describe the cumulative tension damage of the concrete. The allowable value of the dynamic tensile strength of the concrete of the shaft lining $[\sigma_d]$ reflects the capacity of the shaft lining concrete to withstand cumulative damage. Although these concepts have no direct quantitative relation, they possess a positive correlation with each other in values. Based on $\sum D$, which serves as a link, the connection between $[\sigma_d]$ and E_t was established in Figure 8.

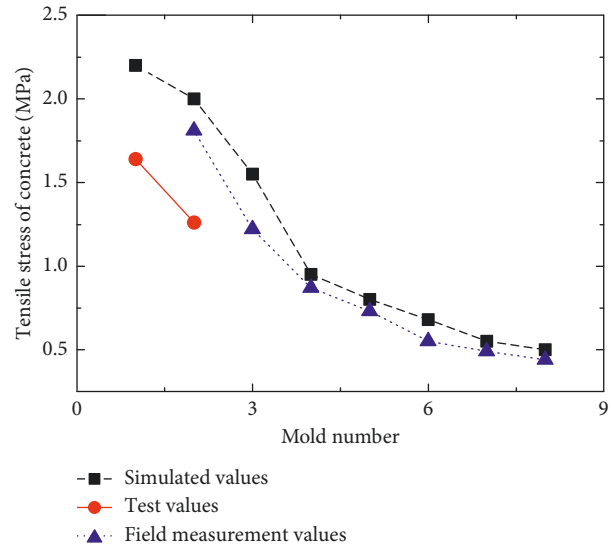

Figure 7: Axial tensile stress comparison among molds of the shaft lining.

To investigate the safety status of each mold shaft lining after being subjected to several rounds of blasting impacts, the net energy and cumulative energy of each mold shaft lining were extracted from the finite element simulation results, and the results are shown in Figure 9. Evidently, with an increase in the distance from the blasting center, the energy of the stress wave attenuates rapidly. The net energy of the eighth mold was less than 5% of that of the first mold. Therefore, the load impacts on each mold of the shaft lining in the ninth round, and subsequent rounds can be neglected, as the cumulative energy sustained by each mold of the shaft lining tends toward stability after the eighth round.

With the continuous excavation of the shaft, the cumulative energy of each mold of the shaft lining increased gradually. However, with an increase in the age of the concrete lining, the dynamic tensile strength of the concrete also increased. Accordingly, the cumulative energy and the allowable dynamic tensile strength were solved for each mold of the shaft lining. For convenience of comparison, the abovementioned quantities were normalized. As shown in Figure 10, the rate of increase of the dynamic tensile strength of the subsequent molds of the shaft linings is greater than that of the cumulative energy. Compared with the first mold of the shaft lining, the safety of the subsequent shaft linings gradually improved. From this perspective, the shaft linings exposed to subsequent rounds of blasting load impacts are safe. In summary, the first shaft lining closest to the heading face will not be damaged upon being exposed to blasting load impacts, and each subsequent mold of the shaft lining will not be damaged after multiple rounds of cumulative loads.

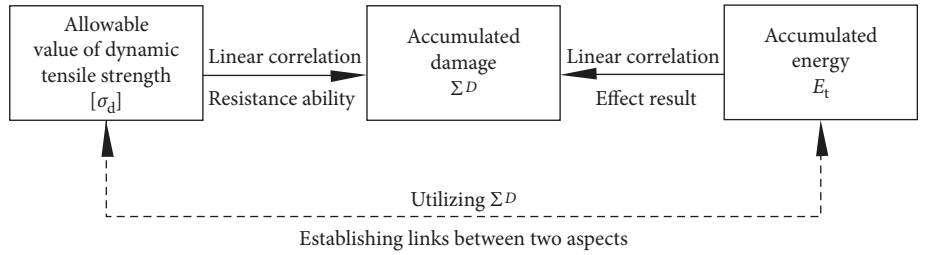

Figure 8: The association between the dynamic tensile strength and cumulative energy of each mold of the shaft lining.

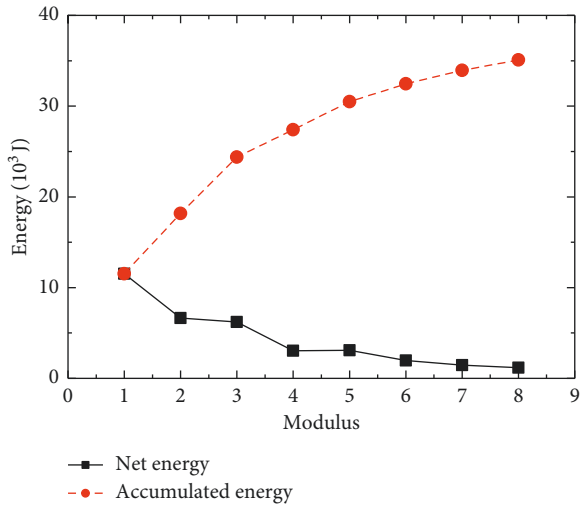

Figure 9: Net energy and accumulated energy for each mold of the shaft lining.

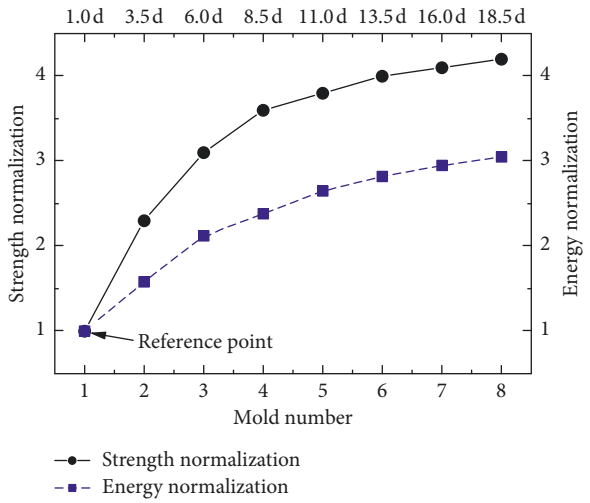

Figure 10: Comparison of the normalized cumulative energy and dynamic tensile strength for each mold of the shaft lining.

Therefore, some unknown factor is responsible for the leakage within the shaft lining, as this phenomenon is not caused by the blasting excavation.

4. Conclusions

This study leads to the following conclusions:

(1) A comparison of the axial vibration velocities and the effective axial tensile stresses of various measurement points reveals that the results of the finite element simulation, in situ measurements, and indoor model test are essentially consistent, attesting to the credibility of the finite element simulation, which can compensate for the failure to monitor the vibrations of the first mold of the shaft lining.

(2) The vertical peak vibration velocity of the first mold of the shaft lining induced by blasting excavation reached 20~25 cm/s, which greatly surpasses the allowable vibration velocity range (i.e., 2~3 cm/s) allowed in the Safety Regulations for Blasting for concrete between the initial setting time and an age of 3 d; the allowable safety coefficient for the axial tensile stress of concrete is 2.3. Therefore, the concrete shaft lining is in a secure state. The velocity limit for the normal strength of concrete in the Safety Regulations for Blasting is somewhat conservative when applied to C65 or higher-strength concrete.

(3) For each mold of the shaft lining, there is a positive correlation between the cumulative damage and the cumulative energy to which it is exposed. The growth rate of the dynamic tensile strength for subsequent mold shaft linings is higher than that of the cumulative energy, indicating that the safety of the shaft lining gradually increases. Consequently, after multiple rounds of blasting impacts, the concrete shaft lining will not be damaged by tensile stresses.

This study investigated only a shaft lining composed of C65 concrete shaft lining in accordance with actual engineering projects. Experiments measuring the vibration velocities of various newly cast high-strength concrete shaft linings exposed to blasting impacts are still scarce, and therefore there is much room for further study.

Data Availability

The data used to support the findings of this study are included within the article.

Conflicts of Interest

The authors declare that they have no conflicts of interest.

Acknowledgments

This study was supported by the Key Project of the Natural Science Foundation of China (51734009), the National Natural Science Foundation of China (51504247), and the China National Building Material Joint Fund Project (2016-m-1).

References

[1] K. F. Unrug, "Shaft design criteria," *International Journal of Mining Engineering*, vol. 2, no. 2, pp. 141–155, 1984.

[2] Z.-s. Yao, H. Chang, and C.-x. Rong, "Research on stress and strength of high strength reinforced concrete drilling shaft lining in thick top soils," *Journal of China University of Mining and Technology*, vol. 17, no. 3, pp. 432–435, 2007.

[3] J.-F. Thimus, "Ground freezing 2000: frost action in soils," in *Proceedings of the International Symposium on Ground Freezing and Frost Action in Soils*, Louvain-la-Neuve, Belgium, September 2000.

[4] T. Han, W. H. Yang, Z. J. Yang, C. Zhang, and D. L. Bo, "Monitoring study of shaft lining concrete strain in freezing water-bearing soft rock during mine shaft construction period in West China," *Procedia Engineering*, vol. 26, pp. 992–1000, 2011.

[5] C. Zhang, F. Hu, and S. Zou, "Effects of blast induced vibrations on the fresh concrete lining of a shaft," *Tunnelling and Underground Space Technology*, vol. 20, no. 4, pp. 356–361, 2005.

[6] X. P. Li, J. Meng, and P. C. Xu, "Study of blasting seismic effects of cable shaft in Xiluodu hydropower station," *Rock and Soil Mechanics*, vol. 32, no. 2, pp. 474–480, 2011.

[7] E. C. Wang, *The damage study of early-age high strength concrete shaft lining subjected to blasting load in northwest freezing shaft*, Ph.D. dissertation, China University of Mining and Technology, Beijing, China, 2014.

[8] R. L. Shan, E. C. Wang, H. Li, J. Y. Cao, Z. L. Li, and L. F. Wei, "Damage model of frozen vertical shaft concrete under blasting load in Northwest China," *Journal of China Coal Society*, vol. 40, pp. 522–527, 2015.

[9] R. L. Shan, L. W. Song, Y. Bai et al., "Model test stumoulds of damage evaluation of frozen rock wall under blasting loads," *Chinese Journal of Rock Mechanics and Engineering*, vol. 33, pp. 1945–1952, 2014.

[10] J. H. Yang, W. B. Lu, Z. G. Zhao, P. Yan, and M. Chen, "Safety distance for secondary shotcrete subjected to blasting vibration in Jinping-II deep-buried tunnels," *Tunnelling and Underground Space Technology*, vol. 43, pp. 123–132, 2014.

[11] N. Jiang and C. Zhou, "Blasting vibration safety criterion for a tunnel liner structure," *Tunnelling and Underground Space Technology*, vol. 32, pp. 52–57, 2012.

[12] W. Jiang, Y. Wang, and Q. Feng, "Study of the influence of blasting load on fresh concrete at adjacent chambers based on DDA," *Procedia Engineering*, vol. 29, pp. 563–567, 2012.

[13] L. Ahmed and A. Ansell, "Structural dynamic and stress wave models for the analysis of shotcrete on rock exposed to blasting," *Engineering Structures*, vol. 35, pp. 11–17, 2012.

[14] L. Ahmed and A. Ansell, "Vibration vulnerability of shotcrete on tunnel walls during construction blasting," *Tunnelling and Underground Space Technology*, vol. 42, pp. 105–111, 2014.

[15] A. Mitelman and D. Elmo, "Analysis of tunnel support design to withstand spalling induced by blasting," *Tunnelling and Underground Space Technology*, vol. 51, pp. 354–361, 2016.

[16] J. Li and H. Hao, "Numerical study of concrete spall damage to blast loads," *International Journal of Impact Engineering*, vol. 68, pp. 41–55, 2014.

[17] SAC, *National Standard of the People's Republic of China: Safety Regulations for Blasting (GB6722-2014)*,Standardization Administration of China, Beijing, China, 2015.

[18] J. R. Del Viso, J. R. Carmona, and G. Ruiz, "Shape and size effects on the compressive strength of high-strength concrete," *Cement and Concrete Research*, vol. 38, no. 3, pp. 386–395, 2008.

[19] D. L. Grote, S. W. Park, and M. Zhou, "Dynamic behavior of concrete at high strain rates and pressures: I. experimental characterization," *International Journal of Impact Engineering*, vol. 25, no. 9, pp. 869–886, 2001.

[20] D. L. Grote, S. W. Park, and M. Zhou, "Dynamic behavior of concrete at high strain rates and pressures: II. numerical simulation," *International Journal of Impact Engineering*, vol. 25, pp. 887–910, 2001.

[21] M. Zhang, H. J. Wu, Q. M. Li, and F. L. Huang, "Further investigation on the dynamic compressive strength enhancement of concrete-like materials based on split Hopkinson pressure bar tests. Part I: experiments," *International Journal of Impact Engineering*, vol. 36, no. 12, pp. 1327–1334, 2009.

[22] Q. M. Li, Y. B. Lu, and H. Meng, "Further investigation on the dynamic compressive strength enhancement of concrete-like materials based on split Hopkinson pressure bar tests. Part II: numerical simulations," *International Journal of Impact Engineering*, vol. 36, no. 12, pp. 1335–1345, 2009.

[23] X. Z. Li, X. Y. Wei, and J. H. Zhao, "Strain rate effect on mechanical properties of concrete," *Journal of Chang'an University (Natural Science Edition)*, vol. 32, pp. 82–86, 2012.

[24] Z. Q. Xu, Q. Yuan, Z. K. Yang, M. M. Wang, and D. Y. Wang, "Mechanical property experiment and uniaxial constitutive model for concrete at early age," *Journal of Shenyang University of Technology*, vol. 37, pp. 92–96, 2015.

[25] Livermore Software Technology Corporation, *LS-DYNA Keyword User's Manual*, Livermore Software Technology Corporation, Livermore, CA, USA, 2007.

[26] T. J. Holmquist, G. R. Johnson, and W. H. Cook, "A computational constitutive model for concrete subjected to large strains, high strain rates, and high pressures," in *Proceedings of the 14th International Symposium on Ballistics*, pp. 591–600, Quebec, Canada, September 1993.

[27] Livermore Software Technology Corporation, *LS-DYNA Theoretical Manual*, Livermore, CA, USA, 1998.